IOP Conf. Series: Materials Science and Engineering **188** (2017) 012021 doi:10.1088/1757-899X/188/1/012021

One-step microwave-assisted colloidal synthesis of hybrid silver oxide/silver nanoparticles: characterization and catalytic study

S P Prakoso[1], A Taufik[1,2] and R Saleh[1,2]

[1]Integrated Laboratory of Energy and Environment, Faculty of Mathematics and Natural Sciences Universitas Indonesia, Kampus UI Depok, Depok 16424, Indonesia
[2]Department of Physics, Faculty of Mathematics and Natural Sciences Universitas Indonesia, Kampus UI Depok, Depok 16424, Indonesia

Corresponding author's e-mail: rosari.saleh@gmail.com

Abstract. This study reports the characterization and catalytic activities of silver-oxide/silver nanoparticles (Ag_2O/Ag NPs) synthesized by microwave-assisted colloidal method in the presence of anionic sodium dodecyl sulfate (SDS) surfactant. To promote different contents of silver in silver oxide, the volume ratio (VR) of ethylene glycol (EG) was varied (VR: 10% to 14%) in relation to the total volume of distilled water solvent. The plasmonic resonance of Ag_2O/Ag NPs could be detected around a wavelength of 350 nm, and it is suggested that Ag_2O/Ag NPs were successfully formed in the colloid solution following exposure to microwaves. Additionally, the growth rate for each crystal phase within Ag_2O and Ag was influenced by an increase of EG as revealed by x-ray diffraction patterns. The morphology, average diameter, and uniformity of Ag_2O/Ag NPs were studied simultaneously by transmission electron microscopy. Infrared absorption measurement of Ag_2O/Ag NPs confirmed the existence of SDS surfactant as a protective agent. Based on the characterization data, Ag_2O/Ag NPs synthesized using this technique exhibited good properties, with high-yield production of NPs. The photocatalytic experiments demonstrate the key role of the crystal phase of Ag_2O/Ag NPs in photocatalytic efficiency.

1. Introduction

Quantum effects in nanoparticles indicate novel properties for future potential applications as distinct from bulk state. Dependency on size, shape, and elements or compounds in nanoscale particles governs alteration of these properties. For instance, the effects of adsorption-desorption on the catalytic process greatly influence the specific surface area of particles even for nanoparticles, as the surface is usually first to interact directly with the "outside world". In addition, the properties of nanoparticles depend on the method used in their preparation. Fazlali *et al.* [1] reported the photocatalytic activity of nickel oxide nanoparticles obtained by various means (thermal-decomposition, sol-gel, hydrothermal, and emulsion nanoreactors), showing differences of performance regardless of particle size. The use of different alkalis (e.g., sodium hydroxide, ammonia solution, urea, and triethanolamine) to obtain nanoparticles through precipitation gives rise to similar phenomena in relation to efficiency of photocatalytic activity [2]. Synthesizing nanoparticles using microwaves has become more popular by virtue of their higher heating efficiency and uniformity as compared to conventional methods of heating such as hot-plate,

heating elements, or heat conduction [3]. Rapid and easy production of nanoparticles using microwaves can be achieved with any suitable method of synthesis.

To date, diverse nanoparticles have been considered in the search for an effective photocatalyst in degrading pollutant organic dyes, which are residual effluents of the textile industry. Of these, oxide semiconductors have attracted interest because of their optical absorption properties, which can be controlled on the basis of gap energies. Silver oxide (Ag_2O) is one of the most suitable oxides for photocatalysis in the visible region, naturally exhibiting p-type conductivity with gap energy (Eg) of around 1.4 eV at room temperature [4]. Despite its good photoabsorption in the visible regions, spontaneous recombination of electron-hole pairs is an issue that hinders the photocatalytic process. To overcome this issue, one technique for inhibiting charge carriers from recombination is to incorporate highly conductive metals to generate localized surface plasmonic resonance (LSPR) effects [5-9]. Along with gold (Au), silver (Ag) is a good metal for generating these LSPR effects [10], and the results of Hu *et al.* [5] demonstrated the extraordinary photocatalytic activities of hybrid Ag_2O/Ag nanoparticles.

Attempts to obtain nanohybrid Ag_2O/Ag particles have included such approaches as co-precipitation and thermal decomposition [5, 8, 9], photochemical reaction [6], and impulse electrochemical deposition [7]. However, to our knowledge, there are few reported studies of the rapid and easy synthesis of controllable amounts of silver in silver oxide nanohybrid particles. The present study reports the characterization and catalytic performance of hybrid Ag_2O/Ag nanoparticles with controlled Ag content as produced in a one-step microwave-assisted colloidal process. To investigate the photodegradation rate of nanohybrid Ag_2O/Ag particles with various Ag contents, methylene blue was employed as a model organic pollutant.

2. Materials and methods

2.1. Synthesis of hybrid Ag_2O/Ag nanoparticles

Production of hybrid Ag_2O/Ag nanoparticles used a household microwave and colloidal synthesis. All precursors were analytical grade reagents, used directly as received and without any further treatment; materials included silver nitrate ($AgNO_3$; Merck), sodium hydroxide (NaOH; Merck), sodium dodecyl sulfate (SDS/$C_{12}H_{25}NaO_4S$; Merck), ethylene glycol (EG/$C_2H_6O_2$; Merck), ethanol, and distilled water. Two solutions (named solution A and solution B) were made prior to starting the reaction. For solution A, a specified amount of $AgNO_3$ was diluted into the 50 mL mixed-solvent, which varied in terms of total volume ratio (VR): 10%, 12%, and 14% EG of 100 mL total volume, making a concentration of 0.09 M. For solution B, 50 mL of distilled water was incorporated by SDS with 1:1 mole ratio to silver ion concentration and an additional 2.6 mL of 2 M NaOH. Solution A was then reacted by solution B under constant stirring for 10 min at room temperature, and this mixed-solution was then irradiated inside the microwave cavity (Electrolux EMM2007X) for 30 sec at an irradiation level of 800 W. The solution was allowed to cool at room temperature while being stirred for 30 min. The precipitate of Ag_2O/Ag was collected by centrifugal force and washed several times with distilled water and ethanol. The final product of Ag_2O/Ag powders was obtained after drying the precipitate at ~120°C for 5 hours in ambient air.

2.2. Characterization methods

The crystal phase of Ag_2O and Ag was examined by x-ray diffraction (XRD) (MiniFlex 600, Rigaku) with an x-ray source operating voltage of 30 kV and a current of 15 mA. Diffraction pattern was recorded within 2θ of 10° to 90°, with a scan step size of 0.02°. Fourier transform infrared (FTIR) measurements were performed using a Shimadzu IR Prestige-21 to confirm the presence of SDS and other possible molecular vibrations in the IR-active region. Potassium bromide (KBr) was employed as a background in recording IR absorption spectra in the 400-4000 cm^{-1} range. Diffuse reflectance spectra (DRS) of UV-Visible were captured by a Shimadzu UV-2450 system, using barium sulfate (Ba_2SO_4) as the baseline correction. The photograph of particle shape was captured by tunneling electron microscopy (TEM) (FEI Tecnai G2 SuperTwin).

2.3. Photocatalytic experiments

Nano-hybrid Ag_2O/Ag catalysts were implemented to degrade methylene blue (MB), which was chosen as a model of organic pollutant in water. A 0.03 g sample of Ag_2O/Ag with varying silver content was dispersed in 100 mL MB solution (20 mg-L^{-1}) at a constant pH of 13. Prior to illumination, the suspensions of Ag_2O/Ag photocatalysts in the MB solution were magnetically stirred in the dark chamber for 30 min to ensure steady state adsorption/desorption of MB on the surface of catalyst particles. The mixtures were then illuminated by 40 W visible light for 120 min. Sampling was repeated every 15 min, and the degraded MB solutions were centrifuged to separate the catalyst. Quantitative analysis of MB in the degraded MB solutions was conducted by UV-Vis spectrophotometer (Hitachi UH5300), which recorded the absorption spectrum in the 450-750 nm range.

3. Results and discussion

The optical absorption spectra of Ag_2O/Ag NPs with various Ag contents are displayed in figure 1. A typical surface plasmonic resonance (SPR) from metallic Ag could be observed at ca. 350 nm [11], suggesting the formation of Ag in Ag_2O for whole samples. While SPR signals became narrower and more intense, the peak position remained unchanged, with increased EG as described in the inset (normalized optical absorption spectra) of figure 1.

The growth of hybrid Ag_2O/Ag NPs with different EG concentrations promoted a variety of Ag loadings, and more EG molecules were drawn to the surface of nanoparticles as revealed by the infrared absorption spectra (see figure 2). Several bands of organic compounds from EG could be identified at 705.9, 883.4, and 1060.9 cm^{-1}, corresponding to C-H bending in plane, C-H stretching mode, and stretching mode of –C=O bonds, respectively [12, 13]. Infrared absorption peaks at 1380.1 cm^{-1} and 1448.6 cm^{-1} were probably caused by the vibration of hydrocarbon groups bonding to Ag clusters [14]. On the other hand, the absorption band at 1663.7 cm^{-1} can be attributed to the –CHO group of acetaldehyde that formed as an outcome of dehydration of EG in the reduction reaction of Ag^+ ions [15]. The appearance of a broad shoulder at ca. 2500-3750 cm^{-1} is associated with the stretching modes of hydrocarbon and hydroxyl groups commonly encountered in oxide semiconductors [13, 16]. Aside from that, the presence of SDS surfactant is barely distinguished. As reported by Ramimoghadam *et al.* [13] the –S=O stretching modes of sulphonic acid groups on the infrared spectrum should occur at around 1027 and 1224 cm^{-1} from pure SDS. It follows that the protective and stabilizing agent from SDS may be diminished during the cleaning process, in contrast to the EG that remains on the nanoparticles.

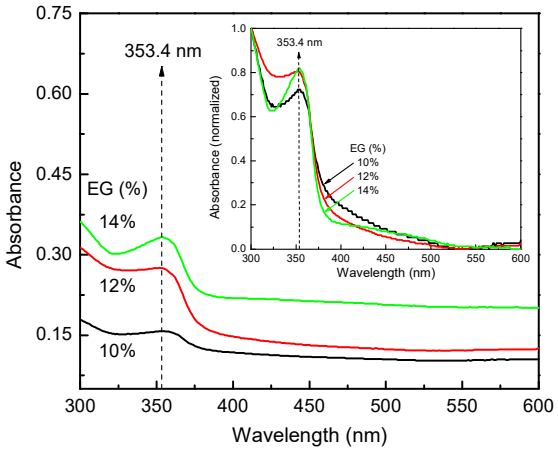

Figure 1. Exhibition of plasmonic resonance from Ag_2O/Ag UV-Vis absorption spectra.

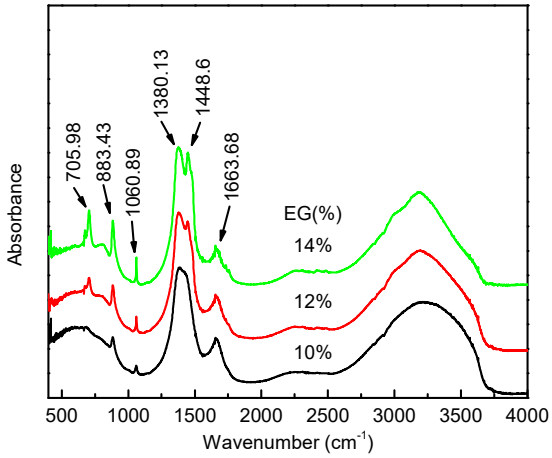

Figure 2. Infrared absorption spectra of hybrid Ag_2O/Ag NPs with various Ag.

Figure 4 shows the diffraction spectra from Ag_2O/Ag NPs with variation of EG volume ratio. Obvious diffraction peaks from cubic-Ag_2O [5] with Pn-3m space group could be indexed at 2θ of 32.5°, 37.8°, 54.6°, and 64.9°, correlated to the (111), (200), (220), and (311) crystallographic planes, respectively. On the other hand, intense growth of cubic-Ag phase (Fm-3m) is clear following the addition of EG from 10% to 14%. The crystal planes of (111) at 37.8° and (200) at 44° can be seen to have grown immensely as compared to the crystal plane of (111) of cubic-Ag_2O phase. Phases other

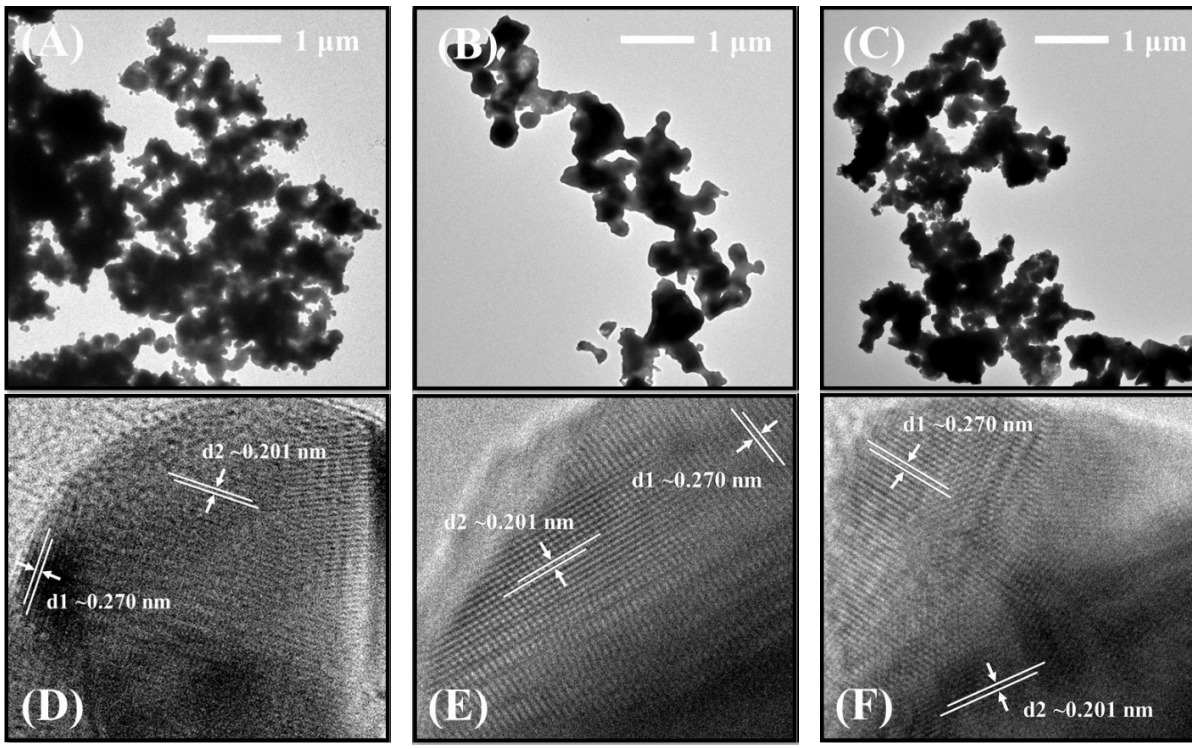

Figure 3. TEM imaging of Ag_2O/Ag NPs grown with 10% (A and D), 12% (B and E) and 14% (C and F) EG.

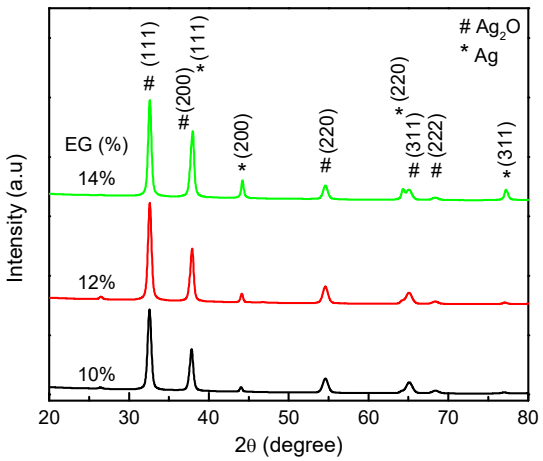

Figure 4. X-ray diffraction spectra of hybrid Ag_2O/Ag NPs grown by various EG concentrations.

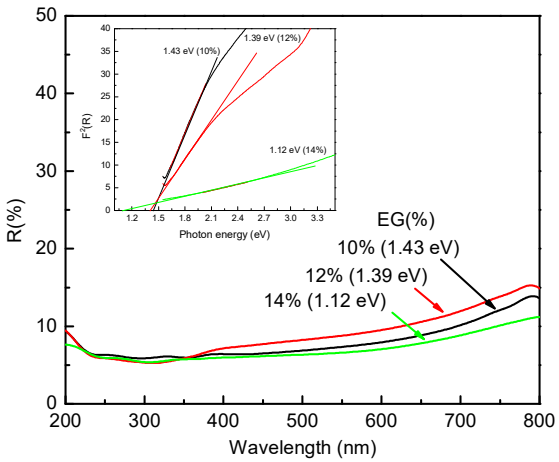

Figure 5. Optical reflectance spectra of various Ag contents in hybrid Ag_2O/Ag NPs.

Table 1. Quantitative analysis of x-ray diffraction patterns from hybrid Ag_2O/Ag NPs.

Crystal Properties	10% EG			12% EG			14% EG		
	Ag_2O (111)	Ag (200)	Ag_2O/Ag (200/111)	Ag_2O (111)	Ag (200)	Ag_2O/Ag (200/111)	Ag_2O (111)	Ag (200)	Ag_2O/Ag (200/111)
<D> (nm)	18.9	30.6	19	19.1	31.1	19.6	21	28.9	18.6
a=b=c (Å)	4.756	4.105	-	4.749	4.101	-	4.744	4.096	-
d-space (Å)	2.75	2.06	2.38	2.75	2.06	2.37	2.75	2.05	2.37
Rel. Intens. (%)	100	6.1	52.02	100	7.76	50.85	100	17.27	75.5
Center (º)	32.56	44.04	37.82	32.59	44.12	37.88	32.59	44.21	37.93
FWHM (º)	0.559	0.4005	0.563	0.553	0.396	0.548	0.515	0.417	0.573
Int. Area (%)	64.39	2.63	32.98	62.67	3.95	33.38	52.48	7.64	39.88

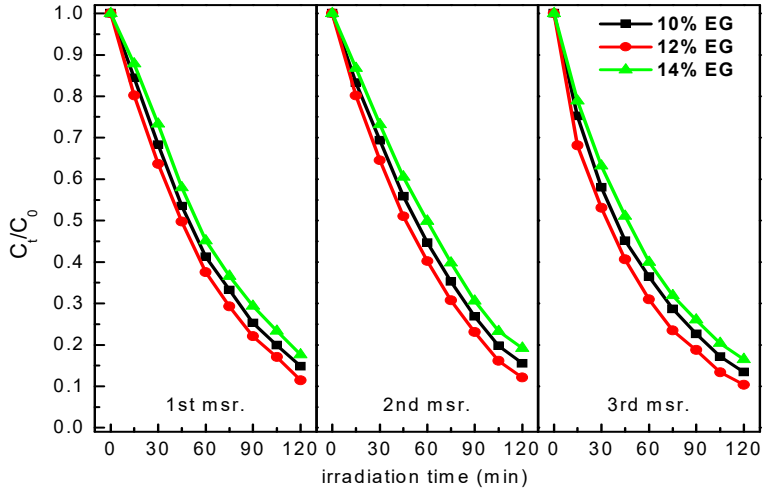

Figure 6. Photodegradation performance of photocatalysts hybrid Ag_2O/Ag NPs with various Ag contents.

than those two were undetectable, which means that the nanoparticles built up solely from Ag_2O and Ag material. Once again, this indicates that the number of Ag clusters can be adjusted by using an appropriate amount of EG in the chemical reaction. Briefly, the calculated average crystallite sizes, lattice parameters, d-spacing, relative intensities, peak centers, full width at half maximum (FWHM), and integrated areas are set out in table 1. According to table 1, several crystal properties are affected by the presence of EG, and the integrated area shows the elevation of Ag phase against Ag_2O phase. However, the crystallite size of Ag phase increases a little (from 10% to 12% EG) and then drops for 14% EG. The computed d-spacing ascribed to (111) plane of Ag_2O phase is about 0.275 nm and 0.206 nm for the (200) plane of Ag phase, as indicated by the TEM images.

To ascertain the optical gap energies of hybrid Ag_2O/Ag NPs with varying Ag content, optical reflectance spectra were recorded (figure 5). Ag_2O/Ag NPs with 14% EG show the lowest reflectance (about 8.84% at 700 nm), insignificantly altered to 11.9% and 10.2% for 12% and 10% EG. These trivial changes in optical reflectance can be attributed to the presence of metallic Ag, as metal tends to strongly absorb light because of SPR generation [10]. As demonstrated in previous studies [16], band gap energies for various Ag_2O/Ag NPs were derived from the reflectance spectra using the Kubelka-Munk function (inset, figure 5). The obtained gap energies were found at 1.43, 1.39, and 1.12 eV, with increased Ag concentration in Ag_2O/Ag NPs. The narrower optical window gap seen in the computed data owes to the electronic structure alteration of Ag_2O following the onset of Ag phase [17]. Similar results have been reported by Huijuan *et al.* [17], indicating that the redshift occurrence caused by different Ag contents can be attributed to change of particle size. The growth of Ag can interfere with the growth rate of Ag_2O, leading to an increase in crystal defects.

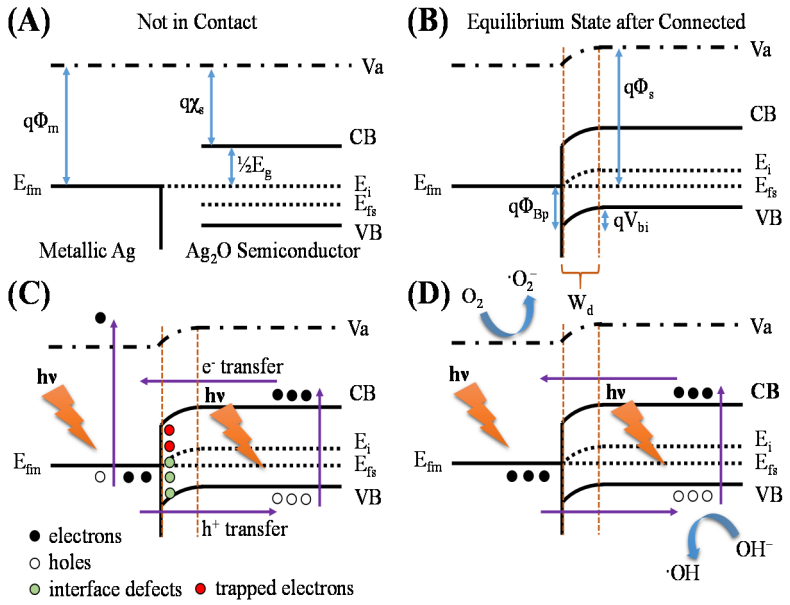

Figure 7. (A and B) Simple schematic of energy band diagrams dwelling on photocatalyst Ag_2O/Ag, (C) possibly charge transport mechanism, and (D) radical groups production process.

Figure 6 displays the photodegradation ability of hybrid Ag_2O/Ag NPs prepared with different EG percentages. Measurements were repeated three times to preserve the reproducibility of photocatalytic activity data. The highest removal of MB under visible light exposure was achieved up to 90% within 120 min with Ag_2O/Ag photocatalyst synthesized with 12% EG. Ag_2O/Ag photocatalyst with 10% and 14% EG reduced MB only up to 87% and 83%, respectively. Reaction rate of photocatalytic performance was estimated from pseudo first-order reaction kinetic studies of linear fitting from the plot of ln (C_0/C_t) vs kt (not shown), where C_0 is initial concentration, C_t is a concentration at time t, and k is a constant rate (min^{-1}) [9]. The observed photodegradation rate for 12% EG was 0.0184 min^{-1}, which is faster than the 10% and 14% EG photocatalyst rates of 0.0164 min^{-1} and 0.015 min^{-1}, respectively. It follows that the photocatalytic activity enhancement occurring in Ag_2O/Ag at 12% EG is probably due to the superior and highly crystalline interfacial contact revealed by x-ray diffraction and TEM imaging analyses [5].

Further corroboration of photodegradation improvement by Ag_2O/Ag is provided by the rough schematic of energy band diagrams in figure 7. To begin, we assume that Ag_2O/Ag NPs consist of metallic Ag and p-type Ag_2O semiconductor where they make Schottky metal-semiconductor contact [18]. Energy bands of isolated metallic Ag and isolated Ag_2O semiconductor are constructed in figure 7a. Upon connection, under thermal equilibrium, these will match each other's Fermi level energy to maintain charge balance. Consequently, a potential barrier (Φ_{Bp}) is formed, together with a depletion layer (W_d) and an upward band bending on the semiconductor side with built-in potential (V_{bi}) (see figure 7b). During visible light exposure, photon energy ($h\upsilon$) excites electrons in the valence band (VB), generating electron-hole pairs in the semiconductor region (see figure 7c), and an SPR effect occurs in the metal region. The photogenerated electrons are further transferred to the metal region owing to the built-in electric field of the Schottky junction and the SPR effect [8]. The photogenerated holes remain on the semiconductor side, as it can interact directly with the dye pollutant and oxidizing water molecules to generate radical groups [9]. Eventually, charge separation is effectively improved where the photogenerated electrons gathered in metal side while the photogenerated holes remain in the semiconductor VB (see figure 7d).

The downgraded photocatalytic activity of Ag_2O/Ag (14% EG) reported here was also reported by Hu *et al.* [5], who noted the influence of a better interfacial contact layer and appropriate size of Ag in

Ag_2O NPs on charge migration, recombination, and charge storage in enhancing photocatalytic activities. In their study, a grain size of Ag phase of about 7-22 nm was the maximum size that could enhance photocatalytic performance, as compared to maximum grain size of Ag phase up to 31.1 nm (Ag_2O/Ag with 12% EG) in the present study. Despite having the highest Ag content in Ag_2O/Ag 14% EG as shown by the integrated area of Ag phase, the calculated grain size is lowest (28.9 nm) as compared to the other samples. Random growth rate and orientation of crystal phase may lead to imperfections and higher defect density. Defects normally increase recombination activities, so preventing charge migration. Linking to the metal-semiconductor contact model, interface defects may account for this issue. Figure 7c demonstrates the scheme case if the interface defect states presence. Such defects may also relate to grain boundary defects [19, 20]. If, for instance, there are several acceptor interface defect centers above Fermi level energy, these centers will be negatively ionized upon capturing the photogenerated electron migration from CB Ag_2O to metallic Ag site (see figure 7c); in consequence, there was a lower photodegradation rate for Ag_2O/Ag produced with 14% EG. Moreover, the TEM images in figure 3d-f offer additional evidence of interfacial/grain boundary defects. Perpendicular crystal orientation among Ag_2O and Ag phase is clearly visible in figures 3d and 3e. For photocatalyst Ag_2O/Ag with 14%, between those phases are inclined rather than perpendicular, probably inducing a larger interfacial defect.

4. Conclusions

In conclusion, various Ag contents of hybrid Ag_2O/Ag nanoparticles were successfully obtained in a one-step microwave-assisted colloidal process. By employing EG as a promoter of reducing agents, different contents of Ag phase within Ag_2O could be controlled, as revealed by diffraction patterns and optical spectra. Infrared absorption showed an increase of EG molecules attached to Ag_2O/Ag particles, along with additional EG concentrations. A specific crystal orientation for Ag_2O and Ag phases was clearly observed in high resolution TEM images. Among Ag_2O/Ag photocatalysts, the one prepared with 12% EG exhibited prominent photodegradation performance towards MB (with a photodegradation rate of 0.0184 min^{-1}). It was posited that the noble metallic Ag improved charge separation through involvement of Schottky junction and SPR effects in the photocatalytic activities of Ag_2O/Ag.

Acknowledgements

Thank you to Hendry Tju who had been assisting in photocatalytic measurements.

References

[1] Fazlali F, Mahjoub A R and Abazari R 2015 *Solid State Sci.* **48** 263-9
[2] Wan X, Yuan M, Tie S and Lan S 2013 *Appl. Surf. Sci.* **277** 40-6
[3] Zhu Y J and Chen F 2014 *Chem. Rev.* **114** 12 6462-555
[4] Ida Y, Watase S, Shinagawa T, Watanabe M, Chigane M, Inaba M, Tasaka A and Izaki M 2008 *Chem. Mater.* **20** 4 1254-6
[5] Hu X, Hu C and Wang R 2015 *Appl. Cata. B: Environ.* **176-177** 637-45
[6] Liu S, Wang N, Zhang Y, Li Y, Han Z and Na P 2015 *J. Hazard Mater.* **284** 171-81
[7] Liu C, Cao C, Luo X and Luo S 2015 *J. Hazard Mater.* **285** 319-24
[8] Chen J, Che H, Huang K, Liu C and Shi W 2016 *Appl. Catal. B: Environ.* **192** 134-44
[9] Umukoro E H, Peleyeju M G, Ngila J C and Arotiba O A 2016 *Solid State Sci.* **51** 66-73
[10] Jia K, Khaywah M Y, Li Y, Bijeon J L, Adam P M, Déturche R, Guelorget B, François M, Louarn G and Ionescu R E 2014 *ACS Appl. Mater. Interfaces* **6** 219-27
[11] Bhui D K, Bar H, Sarkar P, Sahoo G P, De S P and Misra A 2009 *J. Mol. Liq.* **145** 1 33-7
[12] Zhao T, Sun R, Yu S, Zhang Z, Zhou L, Huang H and Du R 2010 *Colloids Surfaces A Physicochem. Eng. Asp.* **366** 197-202
[13] Ramimoghadam D, Hussein Z M and Taufiq-Yap H Y 2012 *Int. J. Mol. Sci.* **13** 13275-93
[14] Slistan-Grijalva A, Herrera-Urbina R, Rivas-Silva J F, Ávalos-Borja M, Castillón-Barraza F F and Posada-Amarillas A 2008 *Mater. Res. Bull.* **43** 90-6
[15] Chen L J, Wan C C and Wang Y Y 2006 *J. Colloid Interface Sci.* **297** 143-50

[16] Prakoso S P and Saleh R 2012 *Mater. Sci. Appl.* **3** 530-7
[17] Bi H, Cai W, Kan C, Zhang L, Martin D and Träger F 2002 *J. Appl. Phys.* **92** 7491-7
[18] Sze S M and Ng K K 2006 *Physics of Semiconductor Devices* (New Jersey: Wiley-Interscience)
[19] Grovenor C R M 1985 *J. Phys. C Solid State Phys.* **18(21)** 4079-120
[20] Ye J D *et al.* 2005 *Appl. Phys.* A **81** 759-62